applied sciences

MDPI

Article

Smart Electronic Device-Based Monitoring of SAR and Temperature Variations in Indoor Human Tissue Interaction

Filippo Laganà [1], Luigi Bibbò [2], Salvatore Calcagno [2], Domenico De Carlo [2], Salvatore A. Pullano [1], Danilo Pratticò [2,*] and Giovanni Angiulli [3]

[1] Laboratory of Biomedical Applications Technologies and Sensors (BATS), Department of Health Science, "Magna Græcia" University, I-88100 Catanzaro, Italy; filippo.lagana@unicz.it (F.L.); pullano@unicz.it (S.A.P.)
[2] DICEAM Department, "Mediterranea" University, I-89122 Reggio Calabria, Italy; luigi.bibbo@unirc.it (L.B.); calcagno@unirc.it (S.C.); domenico.decarlo@unirc.it (D.D.C.)
[3] DIIES Department, "Mediterranea" University, I-89122 Reggio Calabria, Italy; giovanni.angiulli@unirc.it
* Correspondence: danilo.prattico@unirc.it

Abstract: The daily use of devices generating electric and magnetic fields has led to potential human overexposure in home and work environments. This paper assesses the possible effects of electric fields on human health at low and high frequencies. It presents an electronic monitoring device that captures the incidence of specific absorption rate (SAR) and temperature variation (ΔT) on the human body. The system transmits data to a cloud platform, where a feedforward neural network (FFNN) processes the received information. SAR and surface temperature values are detected in an indoor environment, monitoring stationary and moving subjects. The results effectively assess temperature distribution due to electromagnetic fields. The prototype detected temperature peaks and high SAR values when the subjects remained motionless. Predictive analysis confirms the need for workplaces with materials shielding external electromagnetic signals and attenuating internal sources. Moderate mobile phone use could lower SAR and temperature values.

Keywords: electronic monitoring system; infrared thermography; specific absorption rate; biological; FFNN

Academic Editor: Junseop Lee

Received: 25 January 2025
Revised: 19 February 2025
Accepted: 21 February 2025
Published: 25 February 2025

Citation: Laganà, F.; Bibbò, L.; Calcagno, S.; De Carlo, D.; Pullano, S.A.; Pratticò, D.; Angiulli, G. Smart Electronic Device-Based Monitoring of SAR and Temperature Variations in Indoor Human Tissue Interaction. *Appl. Sci.* **2025**, *15*, 2439. https://doi.org/10.3390/app15052439

1. Introduction

The exponential increase in the use of electronic devices and wireless communication technologies has raised concerns about the effects of electromagnetic radiation on human health [1,2]. The research on indoor electromagnetic field (EMF) exposure has focused on measurement techniques, health implications, and mitigation strategies [3–5]. Indoor exposure sources include low-frequency fields (50 Hz) from household electrical networks and broadband electromagnetic fields ranging from 10 to 12 GHz. Wi-Fi routers, mobile devices, and 5G networks are the primary contributors, with enclosed spaces amplifying exposure due to reflection and interference [6,7]. Previous studies have measured exposure levels from these sources, evaluating the specific absorption rate (SAR) and field intensity in different indoor settings [8,9]. Additionally, the research has explored biological effects such as oxidative stress and disruptions in cellular communication [10,11]. Computational modelling has also been used to predict SAR distribution in the human body [12], highlighting the influence of environmental factors, such as building materials and spatial configurations [13]. Indoor exposure levels depend on material composition, spatial arrangements, and the density of electromagnetic sources [14]. Walls, floors, and ceilings influence wave absorption and reflection, affecting how much energy the human

body absorbs [15]. Furniture placement and the presence of multiple radiation sources can lead to scattered or concentrated exposure zones. The movement of individuals also alters electromagnetic coupling, changing SAR distribution in real time. Muscle tissues, due to their conductivity, experience variable absorption depending on ventilation and ambient temperature [16]. SAR is a key metric for assessing EMF safety, as it quantifies the electromagnetic energy absorbed by biological tissues [17]. Thermal effects result from increased tissue temperature, particularly in the brain, where localized heating can affect neuronal activity. Although the increase in temperature is often minimal, long-term exposure raises concerns about cumulative effects [18]. Non-thermal biological effects, such as oxidative stress, altered cellular communication, and potential DNA damage, remain under investigation [19]. Different tissues exhibit varying responses to electromagnetic exposure [20]. The eyes and testicles, for instance, have a limited capacity to dissipate heat, making them particularly vulnerable [21–23]. At high frequencies (e.g., 5G networks), electromagnetic absorption is superficial, affecting the skin. Lower frequencies allow deeper penetration, potentially impacting internal organs. Blood circulation plays a crucial role in dissipating heat, but poorly vascularized areas—such as the eye lens—are more susceptible to overheating [24]. Even small temperature increases (1–2 °C) can disrupt biochemical reactions and cellular homeostasis [25]. Wireless networks, now ubiquitous in homes, workplaces, and public spaces, expose individuals to continuous low-level electromagnetic radiation [26]. Unlike periodic exposure from mobile phone use, Wi-Fi networks operate persistently, radiating electromagnetic fields throughout the day. The research suggests that prolonged exposure may have physiological implications, particularly in confined spaces where electromagnetic waves accumulate [27]. Although numerous studies have shown that there are adverse effects to prolonged exposure to electromagnetic radiation, it is also worth considering the scientific literature that reports the absence of significant impacts on human health under controlled exposure conditions. The evaluation of electromagnetic exposure shows that radiation levels are generally below the safety thresholds set by international bodies, reducing the risk of documented adverse effects [28]. A thorough SAR analysis has shown that most wireless devices are within the established safety limits, with no evidence of adverse health effects [29]. A study analysed measurements of personal exposure to radio-frequency electromagnetic fields and concluded that in most everyday contexts, exposure levels are below the recommended safety limits [30]. Despite international safety regulations, the variability of indoor conditions necessitates individualized assessments to minimize risks. Factors such as the proximity of devices, room layout, and the number of active sources influence SAR levels. Areas with a high electromagnetic density—such as offices with multiple wireless networks—may pose greater exposure risks than open spaces. The existing studies have significantly advanced the understanding of electromagnetic exposure [31]. However, most rely on periodic or simulated measurements, limiting real-time monitoring. Traditional methods often involve bulky laboratory setups or statistical estimations, rather than real-world data collection. Furthermore, the previous research has generally assumed static exposure models, overlooking the dynamic nature of human interaction with EMFs. To address these gaps, this study proposes a continuous monitoring system capable of real-time SAR and temperature tracking. The electronic device integrates sensor-based measurements with artificial intelligence (AI) processing, offering several advantages over conventional methods. Real-time data acquisition, unlike previous studies that rely on snapshots of exposure, is a significant innovation because the proposed system continuously collects SAR and temperature data during various activities. The realized device eliminates the need for bulky laboratory equipment, making it feasible for daily monitoring [32]. The monitoring device detects SAR levels and temperature changes under different indoor conditions. The collected data are transmitted to a

cloud-based artificial intelligence system, where machine learning algorithms process and identify patterns of exposure trends. This study was conducted in a controlled indoor environment, where subjects were monitored both stationary and moving. The experimental conditions included a room size of 4 m × 4 m, with walls designed to reflect typical home and office environments, participating subjects of different body compositions, monitored devices, Wi-Fi routers, cell phones and other electromagnetic sources, and measurement instruments. The feedforward neural network (FFNN) processes sensor inputs, identifies high-risk exposure patterns, and provides predictive information. The results reveal a direct correlation between subject mobility and SAR distribution. Under stationary conditions, hotspots formed in high-exposure areas, particularly near the head and torso. In contrast, movement dispersed SAR concentration, leading to a more even distribution. Higher SAR values were recorded when subjects remained motionless near Wi-Fi routers and mobile devices. Temperature peaks correlated with increased SAR levels, particularly in areas with limited ventilation [33]. Subjects closer to reflective surfaces experienced amplified exposure due to wave accumulation. The AI model accurately classified exposure patterns with a precision of 94%, outperforming traditional statistical approaches. This study demonstrates the feasibility of a real-time SAR and temperature monitoring system enhanced by AI-driven analysis. The findings suggest that adaptive shielding strategies, such as optimized workspace layouts and reduced Wi-Fi usage, could mitigate overexposure risks. By integrating sensor-based monitoring with artificial intelligence, this research advances the understanding of indoor electromagnetic exposure, providing a foundation for improved safety regulations and public health recommendations.

2. Related Works

The interaction between electromagnetic fields (EMFs) and biological systems has been widely studied. Understanding the internal distribution of electric fields, currents, and the rate of energy deposition (i.e., the "dose" of the EMF) is essential for describing this interaction [34]. Computational models have become a key tool in the bio-electromagnetism research, allowing the researchers to quantify EM field distributions and their magnitudes in human tissues. Several studies have focused on the implementation of computational electromagnetic techniques to assess field intensities induced by EMF-based biomedical applications [35,36]. The increasing use of wireless technology in indoor environments has led the researchers to analyse its effects on human exposure. Many studies have monitored stationary subjects sitting in front of computers [37], focusing on two primary parameters: electric field distribution and specific absorption rate (SAR). While these studies contribute to understanding EMF impact, they only address certain aspects of potential health risks [38]. The scientifically established short-term effects of radiofrequency EMFs are thermal in nature, resulting from the conversion of absorbed electromagnetic energy into heat [39]. The increase in body temperature depends on thermoregulation mechanisms, such as increased blood circulation, sweating, and respiration, which limit excessive warming [40]. Studies suggest that body temperature increases below 1 °C are unlikely to have adverse health effects [41]. A widely discussed topic in the scientific community is the comparison of SAR measurements from wireless devices, often using standard dipole antennas and phantom models [42]. SAR evaluations have been validated through intercomparisons of measurements in head phantoms filled with simulant fluid. Studies investigating the impact of 5G networks have focused on millimetre-wave communications in dense indoor environments, analysing whether exposure to higher frequencies could negatively affect human health [43]. One study analysed RF-EMF exposure in high-density environments, such as shopping malls, where Wi-Fi (IEEE 802.11n/ac) and mobile communications (2G–5G) coexist. Measurements were taken in worst-case conditions using deterministic simulations,

demonstrating a good agreement with the experimental data. This research highlights how the coexistence of multiple networks affects overall exposure [44]. The introduction of 6G technology, expected by 2030, has prompted further analysis of distributed multi-input multi-output (D-MIMO) architectures. One study used a hybrid simulation approach combining ray tracing and full-wave simulations for 3.5 GHz indoor transmission. Exposure levels were assessed using incident power density, local SAR, and whole-body SAR [45]. Most studies focus on simplified simulations, neglecting dynamic factors, such as human movement. Additionally, little attention is given to non-thermal effects, despite concerns over potential biochemical alterations due to long-term exposure. Many studies primarily examine tissue heating, overlooking environmental influences, such as the material composition and spatial arrangement of sources, which impact exposure variability. These limitations make it difficult to reproduce results across different indoor settings. Recent years have seen a growing interest in using artificial intelligence (AI) for monitoring body temperature in human tissue [46]. Multimodal sensor analysis has improved diagnostic capabilities, allowing for a more comprehensive assessment of tissue conditions. Machine learning (ML) and deep learning (DL) have been widely applied to analyse complex signals produced by sensors, enhancing the accuracy and efficiency in exposure assessments [47]. Some studies use synthetic datasets based on numerical models of human tissues, training convolutional neural networks (CNNs) to identify anomalies in SAR signals. These models have achieved high diagnostic accuracy. Other studies combine thermal imaging with AI algorithms to track changes in surface temperature, aiding in the early detection of ulcers or infections [48]. This study seeks to address the unresolved gaps by continuously monitoring SAR and body temperature using an integrated electronic system [49].

3. Materials and Methods

The human being is a subject that absorbs signals of any kind; just think about how the power grid, lighting, and electronic devices produce low-frequency signals, while cell phones and wireless modems emit high-frequency signals. Therefore, the domestic and work environments, specifically, must be continuously monitored in order to analyse the electromagnetic signals absorbed by human tissue.

3.1. Scenario of the Incidence of SAR and Temperature Variation on Human Tissues in Indoor Environments

The workplace, with its 33%, represents the most frequented habitat during the day by humans. For this reason, the structural and architectural characteristics actively contribute to achieving high standards of well-being and quality of life, which are crucial for the success of any activity. Among the technical aspects, monitoring the values generated by sources of electromagnetic waves plays an important role in health quality. The scenario monitoring was carried out within an indoor environment (Figure 1) with well-defined architectural elements. In order to solve the problem of signal dissipation [50,51], the area of study and monitoring was reduced, leading the study back to the equivalence theorem of the electromagnetic field theory.

Figure 1 presents two three-dimensional representations of an indoor environment used to study the interaction between Wi-Fi signals and the human body, with the support of SAR sensors for the electromagnetic absorption assessment. Figure 1 depicts in more detail the multi-room environment with walls, doors, and windows. Cartesian axes (x, y, z) define the spatial coordinates, with the numbered scale ranging from 0 to about 4 m along each direction. The presence of an open door (brown) provides a signal interaction with adjacent spaces. This study volume was delimited by yellow lines, indicating the perimeter of signal acquisition and modelling. The Wi-Fi source was strategically placed to assess the

signal distribution in a more realistic environment with obstacles, while SAR sensors were mounted on the walls to detect the electromagnetic field at multiple locations and estimate the specific absorption rate (SAR). Their distribution in multiple lo-cations indicates multi-angle data collection to better understand signal propagation. This study implemented a model divided into two types. The first concerns the measurement of the incidence of SAR and temperature variation on a stationary subject in the room (Figure 2a). The second type involves the study of the incidence of SAR and temperature variation on a moving subject (Figure 2b). Both subjects talked on a 5G technology mobile phone in an enclosed environment where there were sources of low- and high-frequency electromagnetic waves.

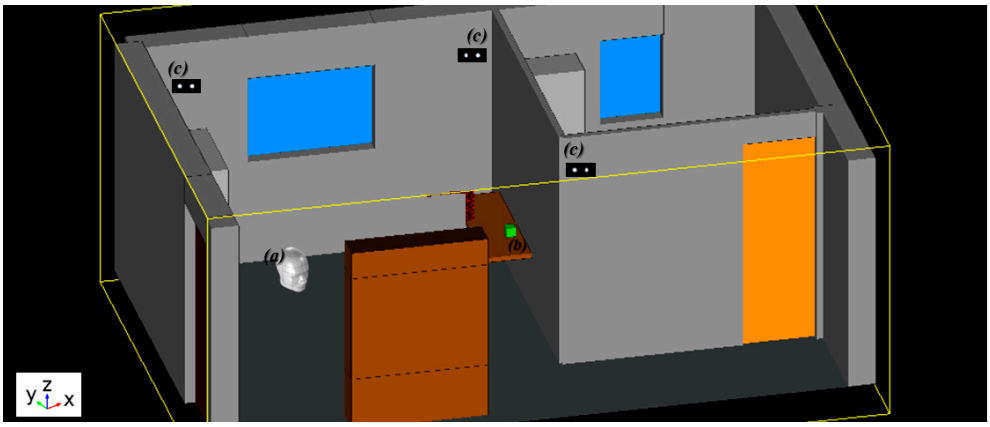

Figure 1. Scenario analysed in indoor environment—(**a**) body area monitored (head); (**b**) Wi-Fi source; (**c**) SAR sensors.

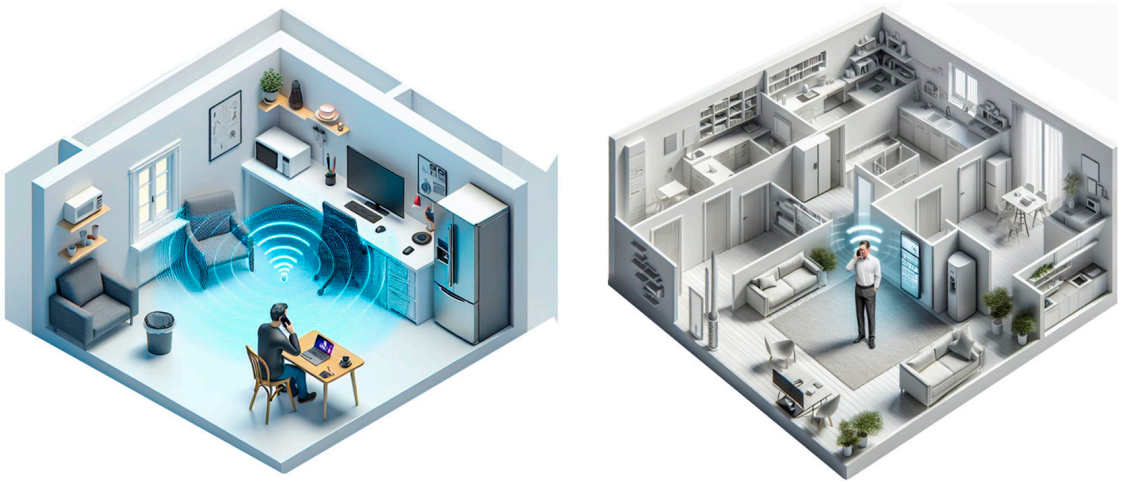

(**a**) (**b**)

Figure 2. Measurement environments: (**a**) stationary subject; (**b**) moving subject.

The International Commission on Non-Ionizing Radiation Protection (ICNIRP) establishes the impact of low- and high-frequency electromagnetic waves on human health, both regarding the electric field and the limits of SAR values created by these electric fields. For frequencies used in mobile telecommunications, the Italian limit is 6 V/m, while the ICNIRP recommends 61 V/m. The SAR limit in Italy, as in many other countries, is 2 W/kg for the head and trunk [52]. Figure 3 shows the variation in the electric field limit values for exposure of the general population established by the ICNIRP and the HHI as a function of frequency.

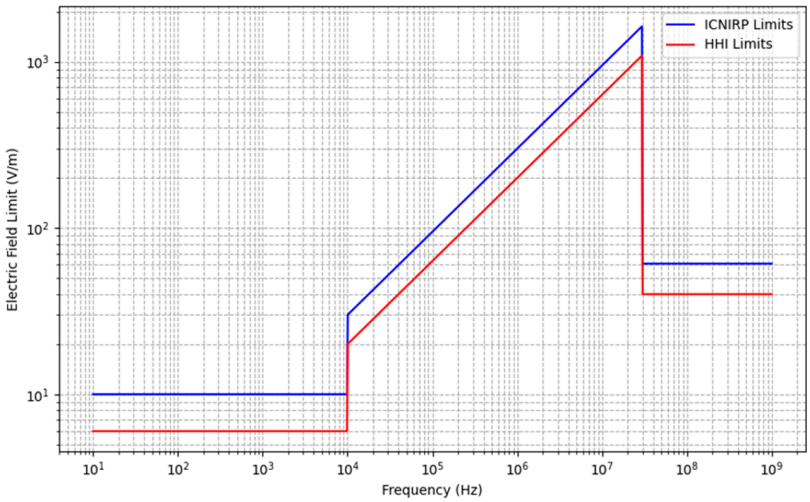

Figure 3. Electric field limit values determined by ICNIRP and HHI for humans.

The impact of frequency on SAR and temperature is crucial, as lower frequencies (e.g., 100 MHz) penetrate tissues more deeply, distributing SAR over a larger volume, while higher frequencies (e.g., 27 GHz) cause localized heating. Heat dissipation depends on blood perfusion and tissue thermal conductivity, with higher frequencies surpassing the dissipation capacity more quickly, leading to greater temperature increases. SAR values were computed using permittivity and electrical conductivity (ε_r, σ), as shown in Table 1 [53]. Lower frequencies result in gradual, diffuse heating, whereas higher frequencies induce rapid, localized temperature rises, affecting tissue response to electromagnetic exposure.

Table 1. Electrical properties of human tissue.

Bands MHz		Skin	Fat	Bone	Brain
LTE 800	ε_r	41.66	5.47	12.51	46.04
805.95	σ	0.83	0.04	0.12	0.73
ETC 1	ε_r	41.44	5.46	12.46	45.84
873	σ	0.84	0.04	0.12	0.73
GSM 900	ε_r	41.26	5.45	12.41	45.67
948.05	σ	0.88	0.05	0.14	0.79
ETC 2	ε_r	40.05	5.39	12.10	44.56
1383.05	σ	1.03	0.06	0.21	0.97
LTE 1800	ε_r	38.83	5.33	11.76	43.32
1849.5	σ	1.20	0.07	0.28	1.17
WLAN	ε_r	38.04	5.28	11.38	42.53
2441.5	σ	1.45	0.10	0.39	1.50
4G	ε_r	38.2	4.8	14.5	48
2600	σ	0.6	0.05	0.025	1.3
5G	ε_r	35	4.5	14	45
26,000	σ	0.7	0.06	0.03	1.4
ρ (density) (Kg/m^3)		1100	920	1850	1030

The limits for SAR values were determined between 10 Hz and 10 GHz, taking 1 g of tissue and 10 g of exposed organ or the whole body as a reference. The value chosen falls within a frequency range where absorbed electromagnetic energy should not cause thermal damage to human tissue. SAR limits were differentiated according to the work environment, which can be indoor or outdoor. Table 2 shows the limits set for the work environment and public areas [54].

Table 2. Electrical characteristics of the developing layers.

	Whole Body Average SAR (W/Kg)	Localized SAR (Head and Trunk) (W/Kg)	Localized SAR (Limbs) (W/Kg)
FCC (1 g)			
Occupational Exposure	0.4	8	20
General Public Exposure	0.08	1.6	4
CE (10 g)			
Occupational Exposure	0.4	10	20
General Public Exposure	0.08	2	4

After determining the electrical properties shown in Tables 1 and 2, which link the interaction of electromagnetic field radiation with human tissue, the electronic system implemented for the acquisition and monitoring of SAR and temperature variation was introduced.

3.2. Electronic System for the Acquisition and Monitoring of SAR and Temperature Variation on Human Tissues

The impact of electromagnetic fields (800 MHz–26 GHz) on human tissues depends on the monitored body area, subject height, and movement within the work environment. To assess these parameters, an integrated hardware/software system was designed for indoor monitoring. The electronic system ensured the effective measurement of specific absorption rate (SAR) and temperature variations. The monitoring device, managed by a Raspberry Pi via the I^2C protocol, acquired and processed sensor data. The SAR sensor, a redundant strain sensor with a LIN bus interface, consisted of strain gauges on a steel support and included a temperature compensation feature. It operated with a 7–18 V power supply, consuming a maximum of 20 mA, within a temperature range of −20 to +70 °C. Its compact size (95 mm × 95 mm × 54.5 mm) allowed flexible application, though in this study, it was not used directly on individuals. Temperature data were captured using an infrared sensor. The Raspberry Pi transmits data to a cloud platform via Wi-Fi, enabling real-time remote monitoring. The system's acquisition and resolution process are outlined in Figure 4, providing a structured approach to SAR and thermal data analysis.

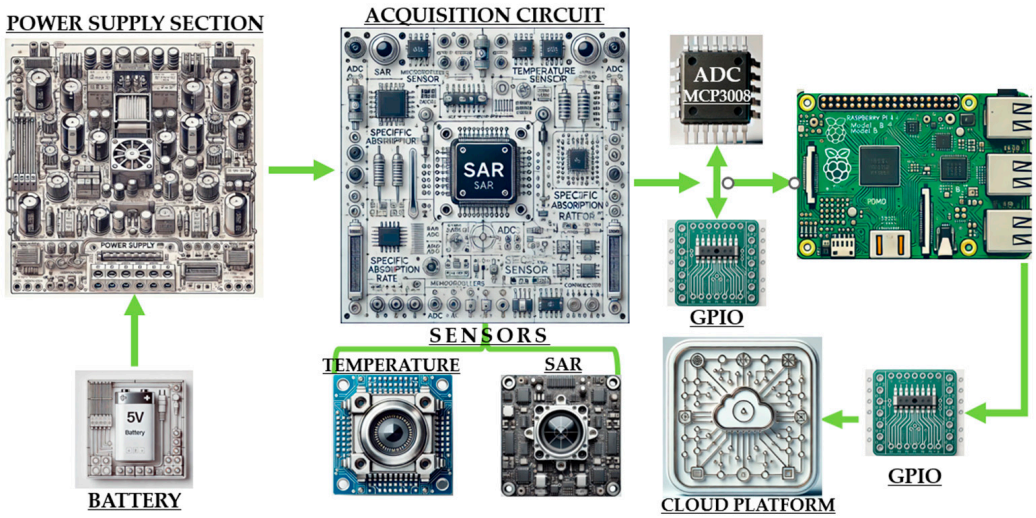

Figure 4. Flowchart monitoring system.

To design the device capable of detecting SAR and body temperature in indoor environments, technologies for electromagnetic and thermal measurement were integrated. The components of the device included a SAR sensor, capable of detecting the absorption rate of electromagnetic field sources up to 26 GHz; a processor to calculate the SAR based on the field intensity and tissue density; an infrared temperature sensor, to measure surface temperature variations; and a Wi-Fi module to transfer the data to a cloud platform where the data were processed with a fully connected feedforward network. The power supply consisted of a rechargeable battery with optimised energy management to ensure portability. The designed device included an acquisition board (Figure 5), interconnected with a Semtech SX9306 SAR sensor and an Omron IR temperature sensor. Semtech SX9306 was selected for its precision in detecting weak signals, enabling proximity and gesture-based monitoring. Its compact size and small package facilitate a seamless integration into the electronic system. The Omron infrared sensor ensures high measurement accuracy, even for minimal temperature variations, and operates effectively in diverse environmental conditions. Its fast response time makes it ideal for monitoring electromagnetic field interference in both stationary and moving subjects. The SAR and temperature sensors use I^2C interfaces for easy integration with the Raspberry Pi microcontroller.

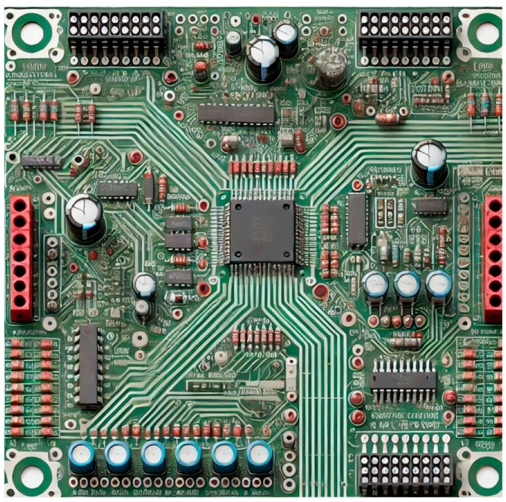

Figure 5. Monitoring board design for SAR and temperature variation signal acquisition.

Designed for a stable performance, the Omron sensor minimizes electromagnetic and optical interference, ensuring reliable readings. The circuit board processes sensor signals by transmitting them to an amplifier that strengthens weak signals and reduces ambient noise. The analogue-to-digital converter (ADC) digitizes the signals and sends them to the Raspberry Pi, where a low-pass filter eliminates high-frequency noise, ensuring clean data acquisition. The Raspberry Pi analyses and displays real-time datum while transmitting it to a cloud platform. A feedforward neural network (FFNN) predicts the effects of SAR interference and temperature variation on human tissues, providing valuable insights for monitoring electromagnetic exposure in indoor environments.

3.3. Post-Processing of SAR and Temperature Variation Signals with the FFNN

Unlike traditional models, which often focus on static exposure conditions, this work considered both stationary and dynamic environments, where real-world motion affects the exposure distribution. This study compared simulated predictions with actual measurements, validating the computational model. The acquired data were processed by a feedforward neural network (FFNN) designed to predict SAR values. The network consists of dense layers with five input variables, structured with 64, 32, and 16 nodes as

hidden layers and one node for continuous SAR prediction as the output rate. By integrating real-time measurements, artificial intelligence-driven analysis, and environmental modelling, this work improves the understanding of electromagnetic exposure and its effects on human health. This research also aims to contribute to new safety guidelines by leveraging artificial intelligence for more accurate exposure assessments. In this study, we developed a feedforward neural network (FFNN) designed for post-processing SAR signals and temperature variations for predictive analysis [55]. The input of the network is an array $x = [x_{SAR}, x_{frequeny}, x_{temperature\ variation}]$ of size $(n_{features})$, where $n_{features}$ is equal to 3, i.e., the number of features. The input of the network is an array size equal to 3, i.e., the number of features. The SLM architecture of the FFNN consisted of 3 nodes and the input values were pre-processed in a range [0, 1]. The hidden layer had a size of 8 nodes and had a rectified linear unit activation function (ReLU), shown in Equation (1).

$$f(x) = max(0, x) \tag{1}$$

The second hidden layer, on the other hand, had a size of 6 nodes and a ReLU. The output layer had a dimension of 2 nodes—temperature predictions and SAR levels—and a linear activation function (Figure 6).

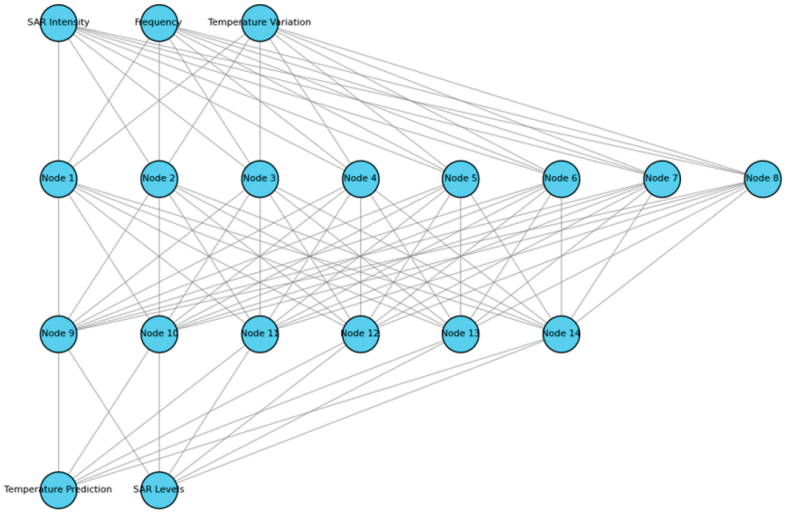

Figure 6. Feedforward neural network architecture.

The dataset used for the training and evaluation of the feedforward network was constructed using data from the two main sensor types, namely the "Semtech SX9306" SAR sensor and the "Omron IR" infrared temperature sensor. The dataset included supervised labels necessary for the network learning process. These labels specifically include numerical values of expected temperatures, expected SAR exposure levels, and qualitative risk classes, such as safe, moderate exposure, and critical exposure. To ensure effective model training and minimize errors or overfitting, the collected data underwent pre-processing. All data were scaled with the MinMax Scaling function to normalize inputs to a [0,1] range to prevent disproportionate influences from different scales (e.g., temperature and SAR intensity). A low-pass filter was applied to SAR signals to attenuate high-frequency interference, while temperature measurements were cleaned of outliers for accurate thermal representation. To enhance generalization and prevent overfitting, data compression was implemented, considering potential signal quality loss. Principal Component Analysis (PCA) was used to transform multidimensional data, retaining key information while discarding less significant variance components.

Figure 7 shows how the steps performed resulted in a clean, scaled, and optimised dataset, ready to be used in feedforward network training. Pre-processing not only improves the quality of the data, but also reduces the risk of overfitting, ensuring the greater predictive ability of the model. The choice of using a FFNN instead of more complex algorithms, like CNN or RNN, was due to the nature of the dataset that consisted of numerical measurements (SAR, temperature, and distance). Each data point represents an independent measurement, meaning there is no need to capture temporal dependencies. The last advantage of the FFNN is the high accuracy with low computational cost, making it suitable for real-time applications. The proposed technique provides accurate predictions, as the network learns directly from the historical data, is flexible, can be adapted for both regression and classification, and, most importantly, can be used for real-time analysis.

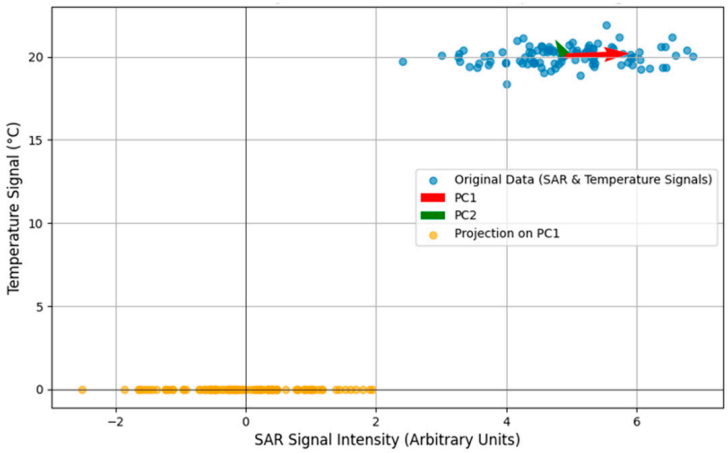

Figure 7. PCA: dimensionality reduction for SAR and temperature signals.

The training phase was carried out using the Mean Squared Error (MSE) as a Loss Function, Adam Optimizer, 32 batch size, and 50 epochs. Dataset split between the training and testing phase was, respectively, an 80–20 ratio.

Framework was implemented with the Tensorflow and Keras library (https://keras.io accessed on 19 September 2024) on Python 3.11.9.

4. Results

The device described measured SAR and temperature values on five volunteers: three men and two women. The accuracy of the measurement made by the device takes into account both the frequency of the signal, the position of the electromagnetic source, the two different types of measurement made (stationary subject, moving subject), and the ambient temperature. The temperature variations measured are influenced by the heat loss coefficient and the blood flow of the subject being monitored, so it varies from case to case. The sensitivity of the sensors is affected by environmental fluctuations, but overall, the device demonstrates high accuracy in measuring SAR and temperature due to the integration of advanced sensors.

Figure 8 shows the comparison between the SAR and temperature values measured by the device and the normative limits, where the solid red line represents the measured temperature values based on the detected SAR, while the dashed red line represents the normative estimate of the temperature variation as a function of SAR. The dotted red line represents the maximum acceptable temperature rise limit (~1 °C), while the dashed blue lines are the SAR regulatory limits defined by the FCC (1.6 W/kg) and EC (2.0 W/kg). The information received, managed by the intelligent System on Module (SOM), is sent to the database, which stores it and makes it available for processing by the FFNN. The

device forwards to the platform the information needed to monitor the incidence of SAR and temperature change on human tissue. The first data monitored and acquired by the device concern the incidence of SAR and temperature variation on human tissue, show in Figure 9a,b. To enhance the clarity and relevance of the figures, we now provide a detailed mathematical framework for calculating the "impact" metric shown on the y-axis.

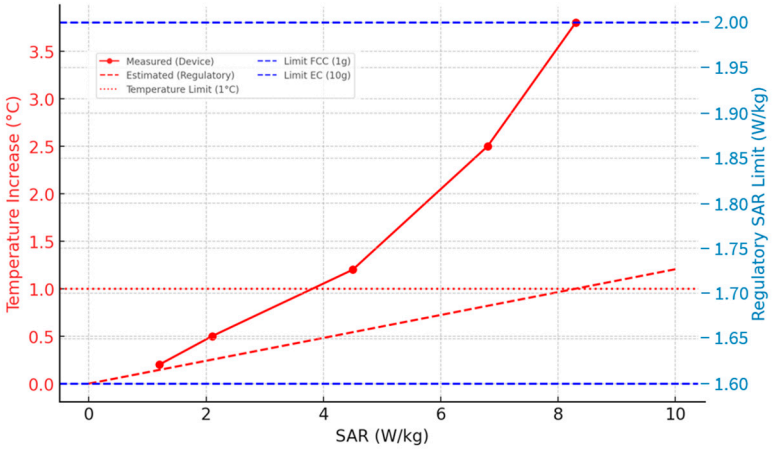

Figure 8. Comparison between the SAR and temperature values measured by the device and the normative limits.

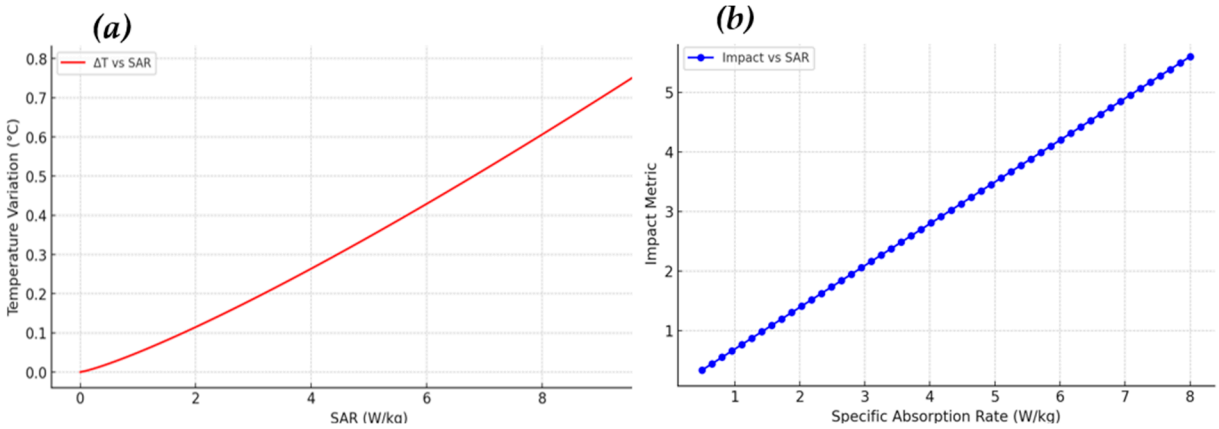

Figure 9. Variation of SAR and temperature on tissues: (**a**) impact in an indoor environment; (**b**) impact of SAR on human tissue as the temperature changes.

The impact is defined as a function of the specific absorption rate (SAR) and the temperature variation (ΔT), which are correlated using empirical data and AI-based predictive modelling. The calculation of the above is determined by Equation (2).

$$IMPACT = f(SAR, \Delta T) = \alpha \cdot SAR + \beta \cdot \Delta T \quad (2)$$

The coefficients α and β represent empirical parameters derived from experimental data and computational modelling, which influence the relative weight of the specific absorption rate (SAR) and temperature variation (ΔT) in the final impact value. The α coefficient considers the sensitivity of biological tissue to electromagnetic absorption and is influenced by factors such as tissue permittivity, conductivity, and penetration depth as a function of frequency. Higher α values indicate a greater susceptibility of tissue to SAR effects. The β coefficient modulates the contribution of temperature change to the overall impact and reflects the thermal dissipation characteristics of the tissue, including blood perfusion and thermal conductivity. A higher β value indicates a greater tissue

response to temperature changes, which can be critical for assessing localized heating effects at high frequencies. Calibrating both coefficients ensure an accurate estimation of the impact and their values are obtained by controlled experiments and optimization techniques based on machine learning. By adjusting α and β, the model can be adapted to different tissue types, exposure conditions, and environmental factors. The SAR is calculated as a function of electromagnetic field strength and electrical properties of human tissue. Omron's infrared sensor measures the change in skin surface temperature due to the absorption of electromagnetic waves. Body temperature is monitored in real time and compared with expected values based on the intensity of exposure.

The curve shows a monotonically increasing trend because the acquired data show the direct, non-linear relationship between SAR and temperature variation. The temperature increase gradually increases for low SAR values, while it becomes more pronounced at higher SAR levels (>6 W/kg). This highlights a potentially exponential behaviour common in thermal dissipation processes on biological materials. Low SAR values (<2 W/kg) correspond to a negligible temperature change, compatible with regulated exposure limits for human safety. At higher SAR levels (>8 W/kg), the temperature rise reaches significant values, which may imply harmful effects or physiological changes in human tissue.

Figure 10a depicts the incidence of SAR on human tissue in relation to the change in ambient temperature, assuming that the temperature in the indoor environment is 20 °C. Considering the different thermal increase scenarios, the curves show an increasing linear trend for all values of temperature variation. The increase in incidence, as shown in the figure, is proportional to the SAR value, becoming more pronounced as the temperature variation increases. As the ambient temperature changes, the incidence increases progressively, implying that this process amplifies the effect of SAR on human tissue. The observed linear trend confirms that the response of human tissue to SAR is modulated by the degree of heating, and the thermal influence can be attributed to increased absorption of electromagnetic waves at elevated temperatures. Another monitored data concern is the variation in temperature on human tissue with changes in the frequency and position of the source in a room measuring 4 m in length, 3 m in width, and 2.7 m in height. The coordinates of the electromagnetic field source on the surface are considered relative to a fixed point, which represents the monitored subject, at a constant height. Set these conditions: the trends in Figure 10b represent the increase in temperature on human tissue as the frequency varies with the source placed at a distance in meters with coordinates (0; 3.3) in blue; (0.7; 1) in orange; (0.8; 0.5) in green; (1.5; 3.9) in red; (2.1; 0.1) in purple; (3.5; 2.5) in brown; (1.3; 1.1) in pink; (3.9; 1.5) in grey; (3.8; 2.9) in golden yellow; and (3.2; 1.9) in light blue.

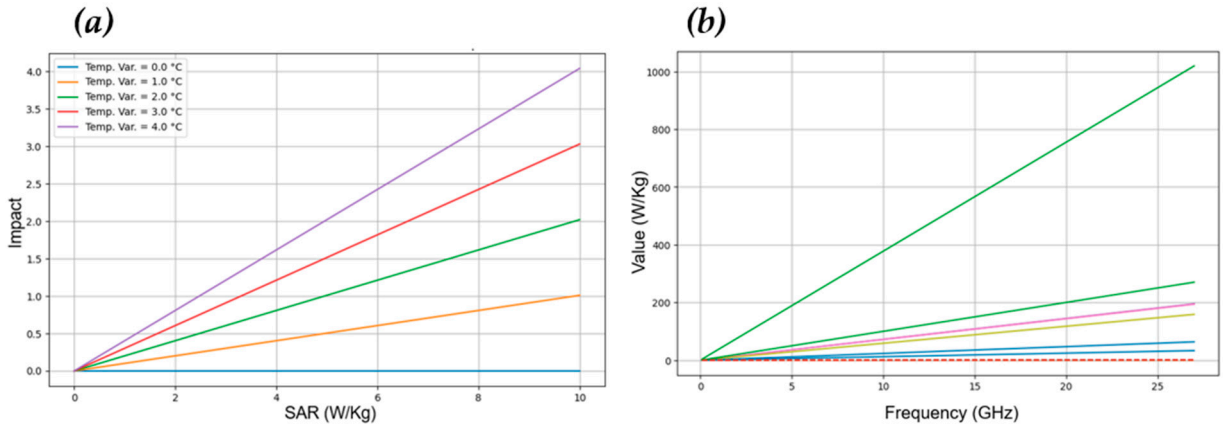

Figure 10. Impact of SAR on human tissue: (**a**) as temperature changes; (**b**) as source frequency changes.

The curves shown in Figure 10b demonstrate how the trend increases as the electromagnetic frequency increases. This implies that the energy absorbed by human tissue increases in direct proportion to the frequency of the electromagnetic waves. At the same time, the temperature increase becomes more pronounced at frequencies above 20 GHz, suggesting greater penetration and absorption at higher frequencies. The results confirm what was expressed in Section 3, i.e., how the proximity and angular position of the source relative to the human tissue significantly influence the absorption of electromagnetic energy and, consequently, the increase in temperature. The latest data monitored and acquired by the device concern the change in SAR and temperature for a moving subject within the indoor environment.

The curves plotted in Figure 11 show two experimental configurations corresponding to distances of 1.0 m and 2.0 m from the electromagnetic source. All curves show an increase in temperature with increasing frequency up to about 10 GHz. Beyond this threshold, a slight reduction in the temperature change is observed due to saturation of the energy absorbed by the human tissue. The logarithmic frequency trend shows that the thermal response of the tissue is closely linked to the interaction between the wavelength of the electromagnetic waves and the dielectric properties of the tissue. Therefore, the distance from the source is a critical parameter for determining the thermal effect. Energy absorption decreases exponentially with distance, consistent with the laws of electromagnetic propagation and field attenuation. The results show that frequency and distance significantly influence the temperature change in human tissue exposed to electromagnetic waves.

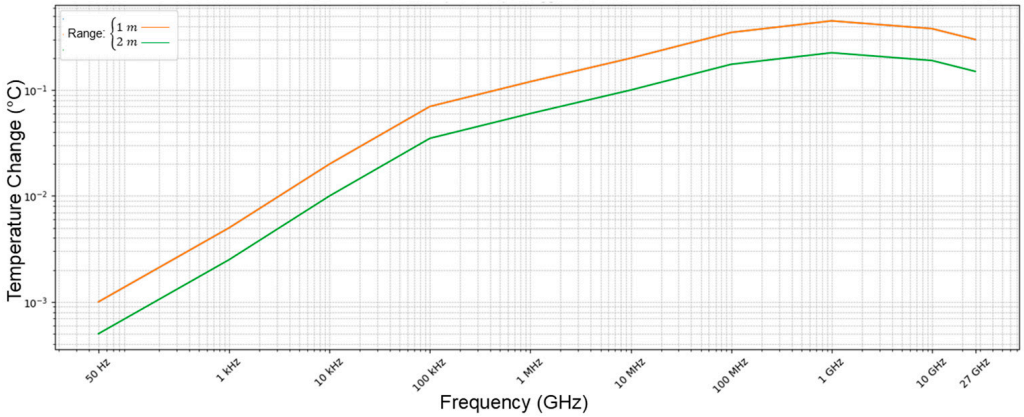

Figure 11. Temperature variation (ΔT) as a function of electromagnetic wave frequency (Hz) for a stationary subject at different distances from the source.

Figure 12 provides a quantitative representation of the energy absorbed per unit mass of biological tissue at varying distances and frequencies, where the decrease in SAR as the distance increases is determined by the inverse of the square of distance. In particular, at higher frequencies, the effect is less pronounced, indicating that energy absorption depends on the penetration of the electromagnetic field into the tissue. In contrast, SAR has low values at frequencies below 1 MHz, regardless of the distance. This behaviour is due to the longer wavelength and lower energy associated with low frequencies. At frequencies above 10 GHz, a decrease in SAR is observed due to the reflection effects of the electromagnetic field on the fabric surface. Maximum absorption occurs in the range of 100 MHz—1 GHz, which is a critical window for biosafety, as the energy absorbed by the tissue is the maximum. SAR decreases significantly with the increasing distance from the source, emphasising the importance of maintaining an adequate distance from electromagnetic sources to reduce exposure. Having generated the cloud-based database of the signals from the SAR and temperature sensors by discriminating the acquisition

variables, we proceeded with the implementation of the FFNN for the prediction of the processed signals. The results obtained are shown in Figure 13.

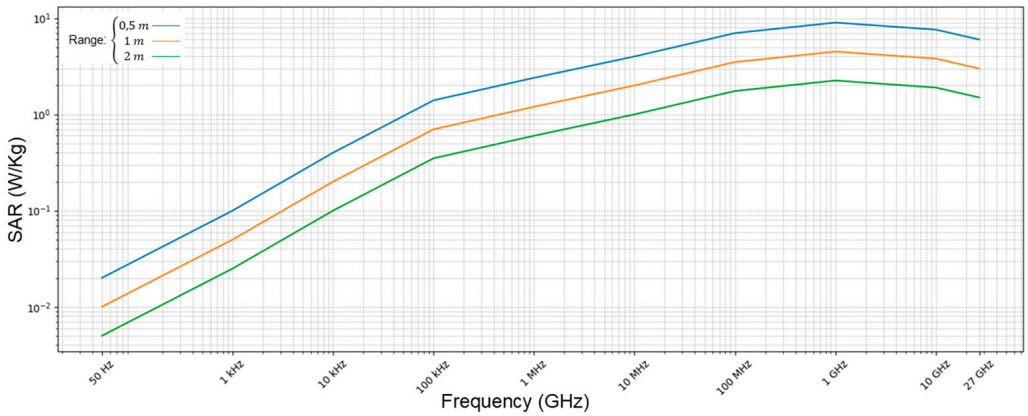

Figure 12. SAR as a function of electromagnetic wave frequency (in GHz) for a subject exposed to electromagnetic sources located at three different distances: 0.5 m, 1.0 m, and 2.0 m.

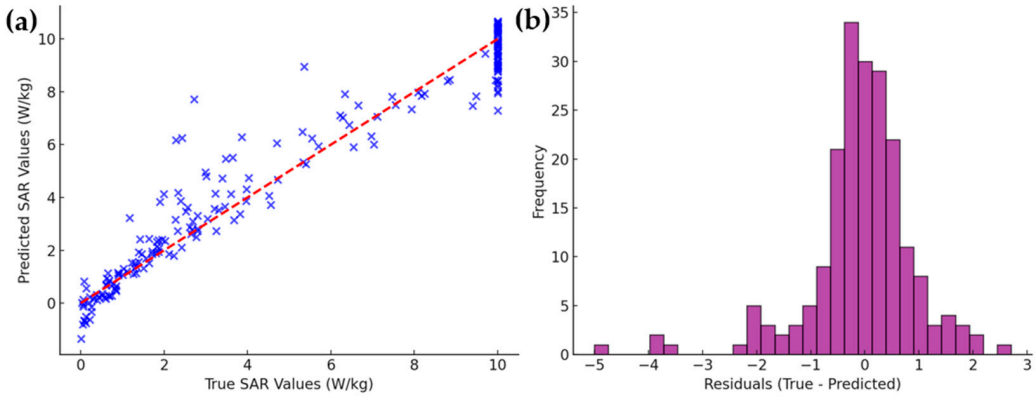

Figure 13. FFNN results: (**a**) true vs. predicted SAR values; (**b**) residuals distribution.

The results of the FFNN demonstrate that the relationship between the actual values and the predicted values, shown in Figure 13a, exhibits a good correspondence. The model maintains a linear relationship, despite the limited deviations from the regression line. Some dispersions occur for higher SAR values, as the model might overestimate or underestimate the extreme values. The distribution of the residuals, shown in Figure 13b, on the other hand, demonstrates the absence of a systematic bias in the model. Most of the residuals fall within the range $[-2, 1]$, which implies limited errors for most predictions. The implemented model shows high overall accuracy, highlighting a good predictive capability for SAR values. To strengthen this study's contribution, we incorporated a comparative analysis with the existing literature on SAR and temperature monitoring in indoor environments. Prior research has examined SAR distribution and thermal effects using computational models and empirical measurements [56–58]. Our study advances this by integrating real-time data acquisition with AI-based processing, improving exposure assessments. The obtained results align with the previous studies on electromagnetic absorption [59,60], but provide novel insights into dynamic human interaction with EMFs.

5. Conclusions

The evaluation and monitoring of temperature variation and SAR in an indoor environment on the human tissue of a stationary and moving subject were the main objectives of the proposed study. Over many years of work, the modelling and measurement of SAR and temperature values on individuals have been the subject of the scientific research.

Based on the strength of the electromagnetic field generated by everyday sources, the analysis of SAR and temperature variation on the human body covers a topic that is not negligible for human health. This consideration has led to meticulous research work, which involved various types of signal measurements and analyses. The results indicate that the tissue regions most vulnerable to temperature changes can be identified using trends based on the source and the subject's behaviour within an indoor environment. Based on the philosophy of the integrated approach, this study involved the development of an electronic device that collects and processes data from SAR sensors and an infrared temperature sensor, as well as the application of a predictive model capable of analysing the acquired signals. The published results underscore how essential real-time data acquisition is. In fact, the acquired signals provide valuable insights into the dynamic interaction between human tissues and electromagnetic exposure in controlled environments. The experimental results validate the performance of the device, confirming its utility in both laboratory and practical applications. Nonetheless, this proposed study identified some objective critical issues, represented by the sensitivity of the sensors to external factors, such as environmental fluctuations, and the accuracy of the calibration. Furthermore, the adaptability of the device to different operational scenarios and its ability to differentiate between various types of fabric and environmental noise require further improvements. For this reason, future research will focus on addressing the identified issues, directing efforts towards improving sensor robustness and enhancing signal processing algorithms to mitigate interference. These advancements aim to establish the device as a reliable tool for broader applications in biomedical research and public health monitoring.

Author Contributions: Conceptualization, F.L., S.A.P., G.A. and D.P.; methodology, F.L., S.A.P., S.C. and L.B.; software, F.L., S.A.P., G.A. and D.P.; validation, F.L., S.A.P., G.A. and S.C.; formal analysis, F.L., S.A.P., G.A. and D.D.C.; investigation, F.L., S.A.P., G.A. and D.D.C.; resources, F.L., S.A.P., G.A. and D.P.; data curation, F.L., S.A.P., G.A. and S.C.; writing—original draft preparation, F.L., D.D.C., G.A. and D.P.; writing—review and editing, F.L., S.C., G.A. and L.B.; visualization, F.L., S.A.P., G.A. and L.B.; supervision, F.L., S.A.P., G.A. and S.C.; project administration, F.L., S.A.P., D.P. and D.D.C.; funding acquisition, F.L., S.A.P., G.A. and S.C. All authors have read and agreed to the published version of the manuscript.

Funding: This research received no external funding.

Institutional Review Board Statement: Not applicable.

Informed Consent Statement: Not applicable.

Data Availability Statement: The data are contained within this article.

Conflicts of Interest: The authors declare no conflicts of interest.

References

1. Jagetia, G.C. Genotoxic effects of electromagnetic field radiations from mobile phones. *Environ. Res.* **2022**, *212*, 113321. [CrossRef] [PubMed]
2. Ishai, P.B.; Davis, D.; Taylor, H.; Birnbaum, L. Problems in evaluating the health impacts of radio frequency radiation. *Environ. Res.* **2024**, *243*, 115038. [CrossRef]
3. Karipidis, K.; Baaken, D.; Loney, T.; Blettner, M.; Brzozek, C.; Elwood, M.; Lagorio, S. The effect of exposure to radiofrequency fields on cancer risk in the general and working population: A systematic review of human observational studies–Part I: Most researched outcomes. *Environ. Int.* **2024**, 108983. [CrossRef] [PubMed]
4. Jing, R.; Jiang, Z.; Tang, X. Advances in Millimeter-Wave Treatment and Its Biological Effects Development. *Int. J. Mol. Sci.* **2024**, *25*, 8638. [CrossRef] [PubMed]
5. Nguyen, N.H.A.; Falagan-Lotsch, P. Mechanistic Insights into the Biological Effects of Engineered Nanomaterials: A Focus on Gold Nanoparticles. *Int. J. Mol. Sci.* **2023**, *24*, 4109. [CrossRef] [PubMed]

6. Mariscotti, A. Assessment of human exposure (including interference to implantable devices) to low-frequency electromagnetic field in modern microgrids, power systems and electric transports. *Energies* **2021**, *14*, 6789. [CrossRef]
7. Razek, A. Assessment of EMF Troubles of Biological and Instrumental Medical Questions and Analysis of Their Compliance with Standards. *Standards* **2023**, *3*, 227–239. [CrossRef]
8. Ramirez-Vazquez, R.; Escobar, I.; Vandenbosch, G.A.; Vargas, F.; Caceres-Monllor, D.A.; Arribas, E. Measurement studies of personal exposure to radiofrequency electromagnetic fields: A systematic review. *Environ. Res.* **2023**, *218*, 114979. [CrossRef]
9. Kim, S.; Sharif, Y.A.; Nasim, I. Human Electromagnetic Field Exposure in Wearable Communications Systems: A Review. *e-Prime Adv. Electr. Eng. Electron. Energy* **2024**, *8*, 100508. [CrossRef]
10. Hu, B.; Ouyang, Y.; Zhao, T.; Wang, Z.; Yan, Q.; Qian, Q.; Wang, S. Antioxidant Hydrogels: Antioxidant Mechanisms, Design Strategies, and Applications in the Treatment of Oxidative Stress-Related Diseases. *Adv. Healthc. Mater.* **2024**, *13*, 2303817. [CrossRef] [PubMed]
11. Sutter, J.; Bruggeman, P.J.; Wigdahl, B.; Krebs, F.C.; Miller, V. Manipulation of Oxidative Stress Responses by Non-Thermal Plasma to Treat Herpes Simplex Virus Type 1 Infection and Disease. *Int. J. Mol. Sci.* **2023**, *24*, 4673. [CrossRef] [PubMed]
12. Isaia, C.; Michaelides, M.P. A Review of Wireless Positioning Techniques and Technologies: From Smart Sensors to 6G. *Signals* **2023**, *4*, 90–136. [CrossRef]
13. Abdul-Al, M.; Amar, A.S.I.; Elfergani, I.; Littlehales, R.; Ojaroudi Parchin, N.; Al-Yasir, Y.; See, C.H.; Zhou, D.; Zainal Abidin, Z.; Alibakhshikenari, M.; et al. Wireless Electromagnetic Radiation Assessment Based on the Specific Absorption Rate (SAR): A Review Case Study. *Electronics* **2022**, *11*, 511. [CrossRef]
14. Davis, D.; Birnbaum, L.; Ben-Ishai, P.; Taylor, H.; Sears, M.; Butler, T.; Scarato, T. Wireless technologies, non-ionizing electromagnetic fields and children: Identifying and reducing health risks. *Curr. Probl. Pediatr. Adolesc. Health Care* **2023**, *53*, 101374. [CrossRef] [PubMed]
15. Hirata, A.; Diao, Y.; Onishi, T.; Sasaki, K.; Ahn, S.; Colombi, D.; Chen, J. Assessment of human exposure to electromagnetic fields: Review and future directions. *IEEE Trans. Electromagn. Compat.* **2021**, *63*, 1619–1630. [CrossRef]
16. Chiaraviglio, L.; Cacciapuoti, A.S.; Di Martino, G.; Fiore, M.; Montesano, M.; Trucchi, D.; Melazzi, N.B. Planning 5G networks under EMF constraints: State of the art and vision. *IEEE Access* **2018**, *6*, 51021–51037. [CrossRef]
17. Majcher, K.; Musiał, M.; Pakos, W.; Różański, A.; Sobótka, M.; Trapko, T. Methods of Protecting Buildings against HPM Radiation—A Review of Materials Absorbing the Energy of Electromagnetic Waves. *Materials* **2020**, *13*, 5509. [CrossRef] [PubMed]
18. Razek, A. Biological and Medical Disturbances Due to Exposure to Fields Emitted by Electromagnetic Energy Devices—A Review. *Energies* **2022**, *15*, 4455. [CrossRef]
19. Babajani, A.; Eftekharinasab, A.; Bekeschus, S.; Mehdian, H.; Vakhshiteh, F.; Madjd, Z. Reactive oxygen species from non-thermal gas plasma (CAP): Implication for targeting cancer stem cells. *Cancer Cell Int.* **2024**, *24*, 344. [CrossRef] [PubMed]
20. Laganà, F.; Pratticò, D.; Angiulli, G.; Oliva, G.; Pullano, S.A.; Versaci, M.; La Foresta, F. Development of an Integrated System of sEMG Signal Acquisition, Processing, and Analysis with AI Techniques. *Signals* **2024**, *5*, 476–493. [CrossRef]
21. Menniti, M.; Oliva, G.; Laganà, F.; Bianco, M.G.; Fiorillo, A.S.; Pullano, S.A. Portable Non-Invasive Ventilator for Homecare and Patients Monitoring System. In Proceedings of the IEEE International Symposium on Medical Measurements and Applications (MeMeA), Jeju, Republic of Korea, 14–16 June 2023; pp. 1–5. [CrossRef]
22. Menniti, M.; Laganà, F.; Oliva, G.; Bianco, M.; Fiorillo, A.S.; Pullano, S.A. Development of Non-Invasive Ventilator for Homecare and Patient Monitoring System. *Electronics* **2024**, *13*, 790. [CrossRef]
23. Moyano, D.B.; Paraiso, D.A.; González-Lezcano, R.A. Possible Effects on Health of Ultrasound Exposure, Risk Factors in the Work Environment and Occupational Safety Review. *Healthcare* **2022**, *10*, 423. [CrossRef] [PubMed]
24. Qianhao, Y.; Zhang, Y.; Wei, J. A comprehensive review of pulsating flow on heat transfer enhancement. *Appl. Therm. Eng.* **2021**, *196*, 117275.
25. Laganà, F.; De Carlo, D.; Calcagno, S.; Pullano, S.A.; Critello, D.; Falcone, F.; Fiorillo, A.S. Computational Model of Cell Deformation Under Fluid Flow Based Rolling. In Proceedings of the E-Health and Bioengineering Conference (EHB), Iasi, Romania, 21–23 November 2019; pp. 1–4. [CrossRef]
26. Fahad, S.; Li, S.; Zhai, Y.; Zhao, C.; Pikramenou, Z.; Wang, M. Luminescence-Based Infrared Thermal Sensors: Comprehensive Insights. *Small* **2024**, *20*, 2304237. [CrossRef]
27. Liang, C.; Yu, F.R. Wireless network virtualization: A survey, some research issues and challenges. *IEEE Commun. Surv. Tutor.* **2014**, *17*, 358–380. [CrossRef]
28. Dürrenberger, G.; Fröhlich, J.; Röösli, M.; Mattsson, M.O. EMF monitoring—Concepts, activities, gaps and options. *Int. J. Environ. Res. Public Health* **2014**, *11*, 9460–9479. [CrossRef]
29. Ferikoğlu, A.; Çerezci, O.; Kahriman, M.; Yener, Ş.Ç. Electromagnetic absorption rate in a multilayer human tissue model exposed to base-station radiation using transmission line analysis. *IEEE Antennas Wirel. Propag. Lett.* **2014**, *13*, 903–906. [CrossRef]

30. Bhatt, C.R.; Thielens, A.; Redmayne, M.; Abramson, M.J.; Billah, B.; Sim, M.R.; Vermeulen, R.; Martens, L.; Joseph, W.; Benke, G. Measuring personal exposure from 900 MHz mobile phone base stations in Australia and Belgium using a novel personal distributed exposimeter. *Environ. Int.* **2016**, *92–93*, 388–397. [CrossRef]
31. Héroux, P.; Belyaev, I.; Chamberlin, K.; Dasdag, S.; De Salles, A.A.A.; Rodriguez, C.E.F.; Hardell, L.; Kelley, E.; Kesari, K.K.; Mallery-Blythe, E. Cell Phone Radiation Exposure Limits and Engineering Solutions. *Int. J. Environ. Res. Public Health* **2023**, *20*, 5398. [CrossRef] [PubMed]
32. Prattico, D.; Laganá, F.; Oliva, G.; Fiorillo, A.S.; Pullano, S.A.; Calcagno, S.; De Carlo, D.; La Foresta, F. Sensors and Integrated Electronic Circuits for Monitoring Machinery on Wastewater Treatment: Artificial Intelligence Approach. In Proceedings of the 2024 IEEE Sensors Applications Symposium (SAS), Naples, Italy, 23–25 July 2024; pp. 1–6. [CrossRef]
33. Laganà, F.; Pellicanò, D.; De Carlo, D.; Pratticò, D.; Calcagno, S. Evaluation and monitoring of SAR and temperature during an indoor Wi-Fi call. In Proceedings of the 2024 International Workshop on Quantum & Biomedical Applications, Technologies, and Sensors (Q-BATS), Durrës, Albania, 10–11 October 2024; pp. 105–110. [CrossRef]
34. Perez, F.P.; Bandeira, J.P.; Perez Chumbiauca, C.N.; Lahiri, D.K.; Morisaki, J.; Rizkalla, M. Multidimensional insights into the repeated electromagnetic field stimulation and biosystems interaction in aging and age-related diseases. *J. Biomed. Sci.* **2022**, *29*, 39.
35. Chittoor, P.K.; Chokkalingam, B.; Mihet-Popa, L. A Review on UAV Wireless Charging: Fundamentals, Applications, Charging Techniques and Standards. *IEEE Access* **2021**, *9*, 69235–69266. [CrossRef]
36. Harris, L.R. Electric Field and SAR Estimation for Multiple Wireless Device Usage in Capsule Environment. In Proceedings of the Wireless Telecommunications Symposium (WTS), Washington, DC, USA, 22–24 April 2020; pp. 1–5. [CrossRef]
37. Laganà, F.; Prattico, D.; De Carlo, D.; Oliva, G.; Pullano, S.A.; Calcagno, S. Engineering Biomedical Problems to Detect Carcinomas: A Tomographic Impedance Approach. *Eng* **2024**, *5*, 1594–1614. [CrossRef]
38. Repacholi, M.H.; Greenebaum, B. Interaction of static and extremely low frequency electric and magnetic fields with living systems: Health effects and research needs. *J. Bioelectromagn. Soc. Soc. Phys. Regul. Biol. Med. Eur. Bioelectromagn. Assoc.* **1999**, *20*, 133–160. [CrossRef]
39. Laganà, F.; De Carlo, D.; Calcagno, S.; Oliva, G.; Pullano, S.A.; Fiorillo, A.S. Modeling of Electrical Impedance Tomography for Carcinoma Detection. In Proceedings of the E-Health and Bioengineering Conference (EHB), Iasi, Romania, 17–18 November 2022; pp. 1–4. [CrossRef]
40. Brites, C.D.; Marin, R.; Suta, M.; Carneiro Neto, A.N.; Ximendes, E.; Jaque, D.; Carlos, L.D. Spotlight on luminescence thermometry: Basics, challenges, and cutting-edge applications. *Adv. Mater.* **2023**, *35*, 2302749. [CrossRef] [PubMed]
41. Filipec, M.; Đurin, M.J. Thermoregulation and Endocrine Response During Exercise in Pregnancy. *Physiologia* **2025**, *5*, 2. [CrossRef]
42. Bazarbekov, I.; Razaque, A.; Ipalakova, M.; Yoo, J.; Assipova, Z.; Almisreb, A. A review of artificial intelligence methods for Alzheimer's disease diagnosis: Insights from neuroimaging to sensor data analysis. *Biomed. Signal Process. Control* **2024**, *92*, 106023. [CrossRef]
43. Rony, M.K.K.; Alamgir, H.M. High temperatures on mental health: Recognizing the association and the need for proactive strategies—A perspective. *Health Sci. Rep.* **2023**, *6*, e1729. [CrossRef] [PubMed]
44. Amitrano, D.; Di Martino, G.; Di Simone, A.; Imperatore, P. Flood Detection with SAR: A Review of Techniques and Datasets. *Remote Sens.* **2024**, *16*, 656. [CrossRef]
45. Basu, D.; Hasan, S.F. Approximating Electromagnetic Exposure in Dense Indoor Environments. In Proceedings of the 15th International Symposium on Wireless Communication Systems (ISWCS), Lisbon, Portugal, 28–31 August 2018; pp. 1–5. [CrossRef]
46. Zhekov, S.S.; Xu, B. Evaluation of EMF Exposure from Distributed MIMO Antennas for 6G in an Industrial Indoor Environment. *IEEE Trans. Electromagn. Compat.* **2024**, 1–15. [CrossRef]
47. Celaya-Echarri, M.; Azpilicueta, L.; Ramos, V.; Lopez-Iturri, P.; Falcone, F. Empirical and Modeling Approach for Environmental Indoor RF-EMF Assessment in Complex High-Node Density Scenarios: Public Shopping Malls Case Study. *IEEE Access* **2021**, *9*, 46755–46775. [CrossRef]
48. Manickam, P.; Mariappan, S.A.; Murugesan, S.M.; Hansda, S.; Kaushik, A.; Shinde, R.; Thipperudraswamy, S.P. Artificial Intelligence (AI) and Internet of Medical Things (IoMT) Assisted Biomedical Systems for Intelligent Healthcare. *Biosensors* **2022**, *12*, 562. [CrossRef] [PubMed]
49. Wang, L. Microwave Imaging and Sensing Techniques for Breast Cancer Detection. *Micromachine* **2023**, *14*, 1462. [CrossRef] [PubMed]
50. Angiulli, G.; Calcagno, S.; De Carlo, D.; Laganá, F.; Versaci, M. Second-Order Parabolic Equation to Model, Analyze, and Forecast Thermal-Stress Distribution in Aircraft Plate Attack Wing–Fuselage. *Mathematics* **2020**, 8. [CrossRef]
51. Molaei, A.M.; Zakeri, B.; Andargoli, S.M.H.; Abbasi, M.A.B.; Fusco, V.; Yurduseven, O. A Comprehensive Review of Direction-of-Arrival Estimation and Localization Approaches in Mixed-Field Sources Scenario. *IEEE Access* **2024**, *12*, 65883–65918. [CrossRef]
52. Wu, L.; Huang, R.; He, X.; Tang, L.; Ma, X. Advances in Machine Learning-Aided Thermal Imaging for Early Detection of Diabetic Foot Ulcers: A Review. *Biosensors* **2024**, *14*, 614. [CrossRef] [PubMed]

53. Razek, A. Assessment and Categorization of Biological Effects and Atypical Symptoms Owing to Exposure to RF Fields from Wireless Energy Devices. *Appl. Sci.* **2023**, *13*, 1265. [CrossRef]
54. Mutlu, M. Evaluation and SAR Analysis of Low Frequency and Broadband Electric Field Exposure Measurement Values in the Home Environment. *Appl. Sci.* **2024**, *14*, 4169. [CrossRef]
55. Alemaryeen, A.; Noghanian, S. A Survey of the Thermal Analysis of Implanted Antennas for Wireless Biomedical Devices. *Micromachines* **2023**, *14*, 1894. [CrossRef] [PubMed]
56. Greenacre, M.; Groenen, P.J.; Hastie, T.; d'Enza, A.I.; Markos, A.; Tuzhilina, E. Principal component analysis. *Nat. Rev. Methods Primers* **2022**, *2*, 100. [CrossRef]
57. Hou, J.; Lee, J.F.; Doherty, S. State-of-the-Art of Eye Tracking in Mobile-Assisted Learning Studies: A Review of Twenty Years of Empirical Studies. *J. Comput. Assist. Learn.* **2025**, *41*, e13118. [CrossRef]
58. Salem, M.A.; Lim, H.S.; Diong, K.S.; Alaghbari, K.A.; Zarakovitis, C.C.; Chien, S.F. Electromagnetic Field-Aware Radio Resource Management for 5G and Beyond: A Survey. *Computers* **2025**, *14*, 51. [CrossRef]
59. Papale, L.G.; Guerrisi, G.; De Santis, D.; Schiavon, G.; Del Frate, F. Satellite Data Potentialities in Solid Waste Landfill Monitoring: Review and Case Studies. *Sensors* **2023**, *23*, 3917. [CrossRef] [PubMed]
60. Elmahaishi, M.F.; Ismail, I.; Muhammad, F.D. A review on electromagnetic microwave absorption properties: Their materials and performance. *J. Mater. Res. Technol.* **2022**, *20*, 2188–2220. [CrossRef]